

Porous Nanosheet Assembly for Macrocyclization and Self-Release

Xin Liu,^{||} Xiaobin Zhou,^{||} Bowen Shen, Yongju Kim, Huaxin Wang, Wanting Pan, Jehan Kim, and Myongsoo Lee*



Cite This: *J. Am. Chem. Soc.* 2020, 142, 1904–1910



Read Online

ACCESS |



Metrics & More

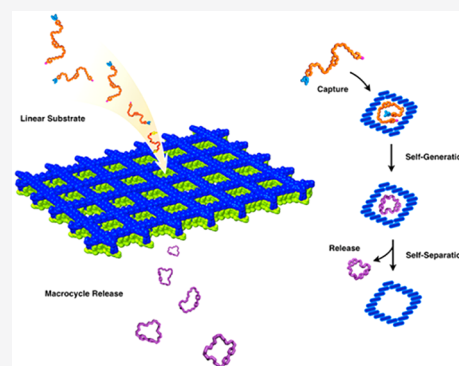


Article Recommendations



Supporting Information

ABSTRACT: Macrocyclic structures are challenging synthetic targets owing to various potential applications ranging from drug discovery to nanomaterials. Their use, however, is highly limited due to synthetic difficulties arising from an entropic penalty for folding of linear chains. Here, we report single-layered porous nanosheets with 2D ordered internal cavities that act as a highly efficient macrocycle generator, changing linear substrates to release as macrocycles in aqueous methanol solution. The nanosheets with hydrophobic cavities encapsulate a linear substrate with nearly perfect uptake, perform clean cyclization, and then spontaneously release as a pure macrocycle. The self-separation of the macrocycle that precipitates from the solution leads to repeated cycles of macrocycle generation; thereby, the single-layered porous materials enabling catch and release offer a powerful novel strategy for repeated macrocycle generation.



INTRODUCTION

Macrocycle topology holds great promise for pursuing challenging targets involved in enhanced bioactivity, selectivity, and stability in the range from drug discovery to nanomaterials.^{1,2} Their use, however, is limited due to synthetic difficulties arising from a prerequisite for a linear precursor to adopt an entropically disfavored, preorganized conformation and prevailed intermolecular reactions.^{3–5} One strategy to overcome these limitations is the confinement of a linear precursor inside a hollow cavity of molecular pore structures such as cages,^{6,7} capsules,⁸ and container molecules.⁹ Constrictive conformations of the linear precursor inside the confined space facilitate efficient cyclization due to the close proximity of the functional ends;^{9–13} however, typically, the molecular pores are far from perfect for cyclization and spontaneous release.

The extended porous nanostructures would be well-fitted to function as molecular containers performing clean cyclization in a confined space;^{14–18} however, the pores are required to be laterally arranged to form a single-layered porous nanosheet structure to preserve a discrete cavity of individual pores without deformation or extension of confined spaces.¹⁹ Single-layered porous materials can be generated by the exfoliation of metal–organic frameworks,²⁰ covalent organic frameworks,^{21,22} the self-assembly of aromatic building blocks,^{23,24} and surface-assisted synthesis.²⁵ Nevertheless, most of the single-layered porous materials are insufficient for clean cyclization due to poor stability in solution caused by strong face-to-face sheet interactions to stack. To prevent sheet stacking, one can introduce flexible chains on the basal plane of the aromatic sheet structures. With this in mind, we designed a self-assembling aromatic building block containing a flexible oligoether dendron that renders isolated self-assembled

structures stable in solution without further aggregation. Here, we report highly stable, single-layered porous nanosheets with in-plane hexagonally ordered hydrophobic internal cavities with a lattice dimension of 4.6 nm that act as a highly efficient macrocycle generator, performing consecutive cycles of changing a linear substrate completely to release as a macrocycle through repetitive substrate catch in aqueous methanol solution at room temperature (Figure 1).

RESULTS AND DISCUSSION

Molecular Design and Self-Assembled Porous Structure. The molecule that forms a single-layered porous nanosheet structure consists of a hydrophilic oligoether dendron and a paired bent-shaped aromatic segment (Figure 1a). Previously, we reported that a bent-shaped aromatic segment with a hydrophilic dendrimer grafted at its apex self-assembles into a hexameric macrocycle that stacks on top of each other to form hollow tubes.²⁶ Based on our previous results, we envisioned that an increased volume fraction of the aromatic segment relative to the flexible chain drives curved structures to transform into planar nanostructures with in-plane ordered pores, similar to the structural transformation in the block copolymer assembly.²⁷ Indeed, self-assembling molecule **1** (Figures S1 and S2) based on a paired aromatic segment leads to a single-layered porous structure in a mixed

Received: October 12, 2019

Published: January 11, 2020



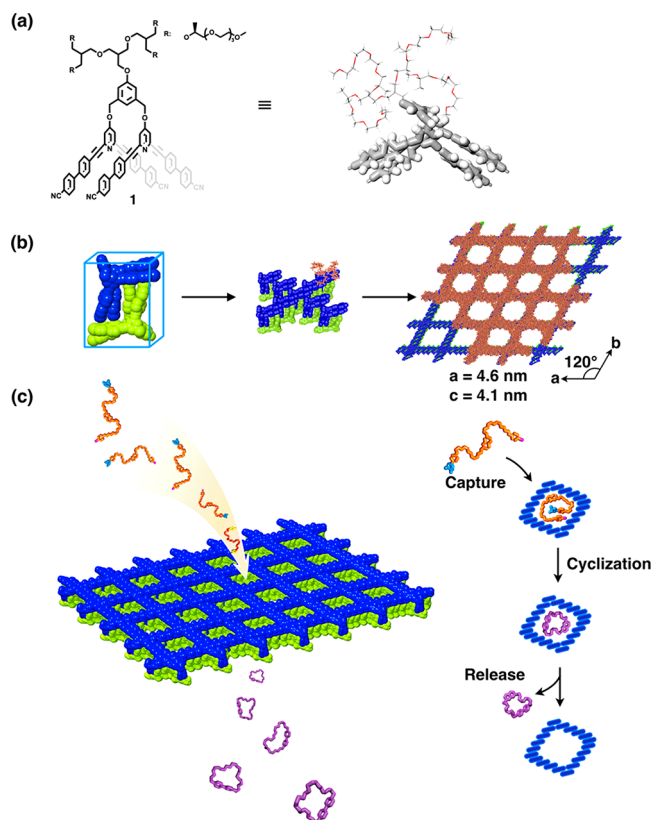


Figure 1. Self-assembly of single-layered porous nanosheets as a macrocycle generator. (a) Molecular structure of **1**. (b) Schematic representation for the formation of a single-layered porous nanosheet with a hexagonal lattice through aromatic stacks of the faced dimers of **1** into branched fibers as an intermediate structure in aqueous methanol solution. (c) Schematic representation of a single-layered porous nanosheet that changes a linear substrate to release as a macrocycle. Dendrimer parts from the porous structure are omitted for clarity.

solution of water and methanol (3/7, v/v). Cryogenic transmission electron microscopy (cryo-TEM) of the structures using a frozen bulk solution of **1** showed large-area nanosheets with straight edges, ranging in their lateral dimensions from submicrometer to several micrometers (Figure 2a), indicating that the nanosheets are robust and freestanding in bulk solution. The inset image revealed hexagonally ordered light spots in a dark matrix, indicative of in-plane ordered hollow cavities in solution (Figure S11). The formation of stable 2D sheet structures in the solution state was further confirmed by fluorescence optical microscopy (FOM), which showed large-area, flat sheet objects (Figure S12). TEM experiments performed with cast films revealed flat 2D structures with straight edges (Figure 2b), consistent with the cryo-TEM results. A high-resolution image revealed a regular framework superstructure with hexagonally ordered pores (Figure 2c and Figure S13). Selected area electron diffraction (SAED) showed bright spot patterns corresponding to a hexagonally ordered single-crystal domain with a lattice dimension of 4.6 nm (Figure 2d). Atomic force microscopy (AFM) analysis showed that the nanosheets are very flat and uniform with a thickness of 4.1 nm (Figure 2e). The magnified image showed that the nanosheet consists of in-plane 2D hexagonal array of the pores, consistent with the results observed from TEM.

Considering the molecular size of **1**, the nanosheet thickness suggests that the primary structure consists of two molecules in which the aromatic segments face one another. When diluted, TEM showed the formation of discrete micelles associated with dimers that self-assemble into crossed nanofibers with slipped packing arrangements (Figure S14). With increasing concentration, the crossed nanofibers are interconnected with each other to form a 2D framework structure. This observation corroborates that the framework consists of intersecting nanofibers in which the crossing points are organized in a 2D hexagonal lattice with a dimension of 4.6 nm. Taking all the data together, we propose that the single-layered porous structure is composed of 2-dimensionally intersected nanofibers to form freestanding, single-layered porous crystalline nanosheets with a thickness of 4.1 nm with an in-plane hexagonal array of the pores (Figure 1b).

To gain more insight into the 2D nanosheet structure, X-ray experiments were performed with freeze-dried samples. Small-angle X-ray scatterings showed several sharp reflections that can be indexed as a hexagonal lattice with dimensions of $a = 4.6$ nm and $c = 4.1$ nm (Figure 2f and Table S1), indicating that the single-layered porous nanosheets with a thickness of 4.1 nm are stacked in an eclipsed AA fashion.²⁸ These dimensions are in excellent agreement with those of SAED and AFM, respectively. The wide-angle X-ray diffraction pattern shows a number of sharp reflections which can be indexed as a face-centered rectangular lattice with unit cell dimensions of $a = 1.61$ nm and $b = 0.92$ nm (Figure 2h and Figure S15), indicating that the dimers are stacked along the framework axis with an interdimer distance of 0.46 nm (Figure 2i). On the basis of these results, and the measured density, the number of molecules consisting of a pore could be estimated to be 18 (Table S2), giving rise to a rhombus-shaped aromatic cavity with dimensions of ~ 2.2 nm in diameter and ~ 2 nm in depth (Figure 2g).

Linear Substrate Binding. We hypothesized that the pores with aromatic internal cavities of such dimensions can sufficiently entrap a linear hydrophobic substrate to adopt a constrictive conformation in hydrophilic solution, a favorable shape for cyclization (Figure 3b). To explore the capability of the porous nanosheets for entrapping a linear substrate, hydrophobic **R1** (Figure 3a and Figure S3) was selected because its estimated size in a constrictive conformation of 2.0 nm is compatible with the internal cavity (Table S3 and Figure S19). Considering that a single pore consists of 18 molecules of **1**, titration experiments showed that each pore is occupied by a single **R1** molecule with greater than 96% uptake of the pores, indicative of the near-perfect fit between the internal cavity and the **R1** substrate (Figure 3c and Figure S16). This provides evidence that the 2D pore array preserves individual porosity without compromising the pore performance for guest uptake. NMR experiments showed the resonance peaks associated with the aromatic protons of the reactant in the porous solution. Considering that the pure reactant in the experimental condition ($\text{H}_2\text{O}/\text{MeOH}$ mixture solution) does not show any peaks associated with the aromatic protons due to the solubility limitation, this result provides clear evidence that the reactant is entrapped in the pore through host–guest interactions (Figure 3d and Figure S17).^{29,30} This coupling was further confirmed by fluorescence enhancement at 374 nm on encapsulating the guests (Figure S18), which could be attributed to the more restricted rotation of the phenyl groups on the aromatic backbone.³¹ To evaluate the uptake of the

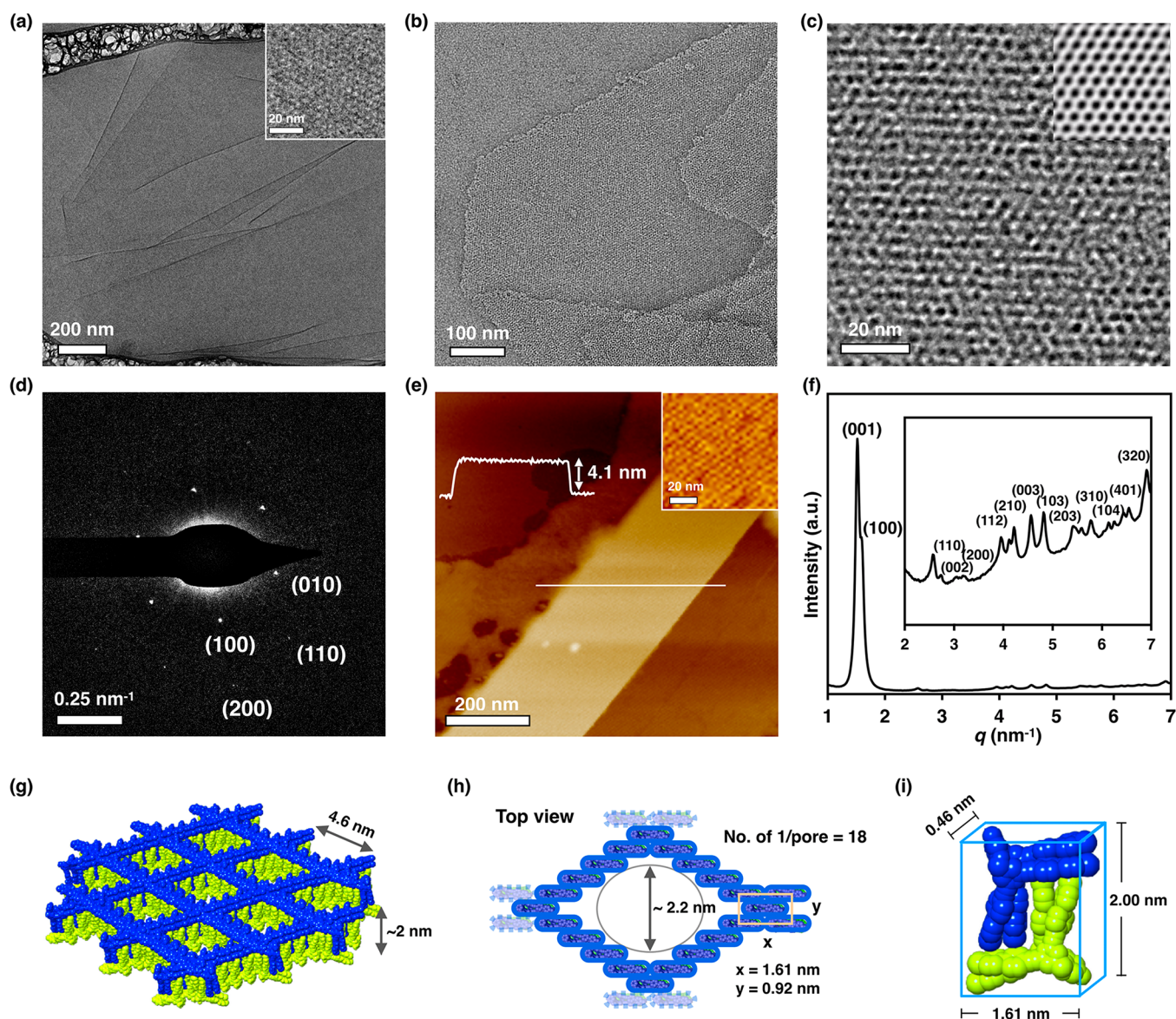


Figure 2. Structural characterization of single-layered porous nanosheets. (a) Cryo-TEM image of **1** ($91 \mu\text{M}$) in water–methanol solution (3/7, v/v). Inset: high-resolution cryo-TEM image showing 2D hexagonal order. (b) Negatively stained TEM image of **1** ($91 \mu\text{M}$) in water–methanol solution (3/7, v/v). (c) High-resolution TEM image of hexagonally ordered pores formed by **1**. Inset: 2D fast Fourier transform image of a hexagonal structure. (d) Selected area electron diffraction pattern of the hexagonal lattice showing $\{100\}$ and $\{110\}$ reflections from $[001]$ projection. (e) AFM height image of the film on a mica surface from evaporation of **1** ($91 \mu\text{M}$) in water–methanol solution (3/7, v/v). The cross-sectional profile (top) is taken along the white line. Inset: magnified image showing 2D hexagonal array of pores. (f) SAXS pattern of **1** with freeze-dried sample. (g) Schematic illustration of aromatic framework with a hexagonal lattice dimension of 4.6 nm and ~ 2 nm in height. (h) Top view of one pore consisting of 18 molecules of **1** with an internal cavity of ~ 2.2 nm in diameter. The cross point on the right-hand side shows a face-centered rectangular lattice with dimensions of $a = 1.61$ nm and $b = 0.92$ nm. One subunit corresponds to the top view of the faced dimer of **1**. (i) Calculated dimensions of a faced dimer of **1** based on WAXS results.

nanosheets with different substrates, we carried out the same experiments with **R2** (Figure 3a and Figure S4) ($d = 1.9$ nm) based on a linear chain (Table S3 and Figure S19). Similar to **R1**, the uptake capacity of **R2** was found to be nearly perfect with an uptake capacity of $>95\%$ occupied pores (Figure S16). In sharp contrast, the nanosheets do not exhibit apparent inclusion activity for the substrates such as **R3** (Figure 3a, Table S3 and Figures S5 and S19) ($d = 1.3$ nm) and **R4** (Figure 3a, Table S3 and Figures S6 and S19) ($d = 2.3$ nm) that are not fitted into the cavity. The clear-cut selectivity in size and the nearly perfect uptake capacity indicate that the

lateral arrangement of the pores into a single layer preserves the pore performance of individual pores in guest uptake.

Macrocyclization of the Linear Substrates. Considering that the end parts of the substrates are functionalized for a Suzuki–Miyaura coupling reaction (Figure 3a), the internal cavities of the pores would function as a molecular container for the open substrates to adopt a preorganized conformation, thus promoting cyclization inside the confined space (Figure 4a).⁹ Moreover, sequestering the substrates would prevent any possible intermolecular processes producing undesired linear oligomers. To corroborate the aromatic coupling cyclization inside the internal cavities, we added a catalytic amount of

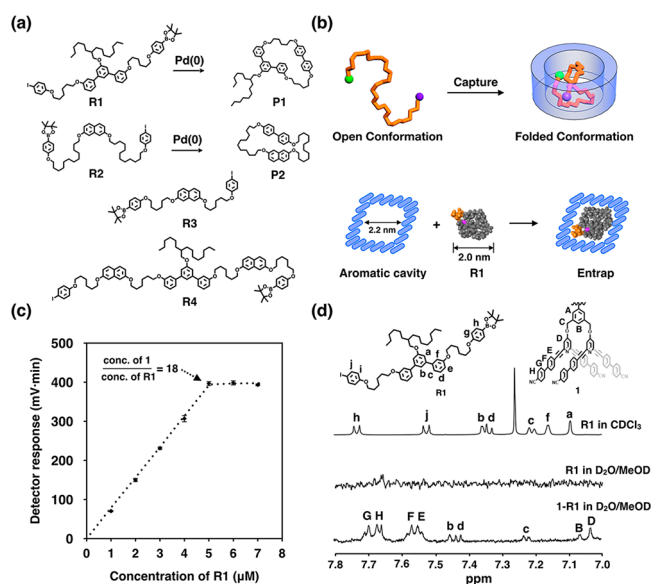


Figure 3. Uptake of linear substrates in porous nanosheets. (a) Chemical structure of linear substrates and macrocycle products. (b) Top: schematic representation of an open chain conformation in a free state and a constrictive conformation inside a confined space. Bottom: R1 with a constrictive conformation fits into the pore cavity to be entrapped through hydrophobic interactions. (c) Substrate uptake as a function of R1 in water–methanol solution (3/7, v/v) at the constant concentration of 1 (91 μM). The saturated concentration of R1 is shown to be 5 μM. Considering one pore consisting of 18 molecules of 1, the saturated concentration of R1 (5 μM) indicates that one pore includes one substrate. (d) ¹H NMR of R1 in CDCl₃, R1 (50 μM) with 1 (912 μM) and without 1 in D₂O-methanol-*d*₄ mixture (3/7, v/v).

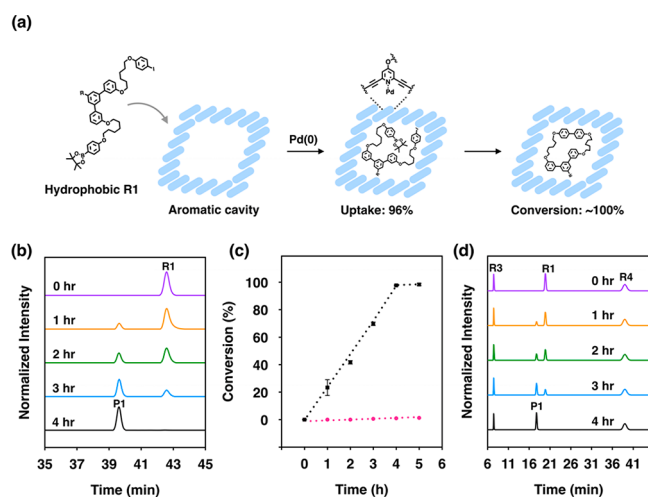


Figure 4. Cyclization of linear substrates in porous nanosheets. (a) Schematic representation of the encapsulation of reactant R1 by aromatic pore and the subsequent macrocyclization with addition of Pd(0) leading to macrocycle product. Pd(0) is complexed with the pyridine units of the pore frameworks. (b) HPLC chromatograms of macrocyclization of R1 in the porous nanosheets of 1 with time variation. (c) Conversion of R1 in the presence of 1 (91 μM) in water–methanol mixture (3/7, v/v) (black ■) and without 1 in toluene/EtOH (pink ●). (d) HPLC chromatograms of selective macrocyclization of a mixture solution of R1, R3, and R4 in the porous nanosheets of 1 with time variation.

Pd(0) (1 mol % relative to R1) to the aqueous methanol solution of 1 (water/methanol = 3/7, v/v) containing R1 at room temperature, which is bound to a pyridine unit of 1 through coordination interactions (Figure 4b and Figure S20).³² Remarkably, the 2D nanoporous sheets perform perfect cyclization of the linear substrate preventing undesired oligomerization at room temperature. Upon addition of Pd(0), only a single additional peak corresponding to a macrocycle product was identified in analytical HPLC of which the intensity increases gradually at the expense of R1 and then levels off at 4 h (Figure 4b). The result indicates that the cyclization of the substrates is completed over 4 h (Figure 4c and Figure S8), while preventing intermolecular oligomerization.

For a control experiment, we performed an identical Suzuki coupling reaction of R1 in toluene/EtOH. In the absence of the porous nanosheets, the coupling reaction did not yield any noticeable reaction products within 4 h even at 75 °C (Figure 4c), indicating that the encapsulation inside the pores accelerate the aromatic coupling reaction. When the toluene/EtOH solution is heated to 75 °C, the reaction takes place very slowly and is completed over 48 h (Figure S21). Nevertheless, the reaction yielded predominantly linear oligomers with only a tiny amount of the macrocycle product (~1 mol %), demonstrating that the inclusion of the open chains inside the internal cavities is essential for perfect cyclization. Accelerating the reaction inside the pores could be attributed to close proximity between the functional groups caused by adopting a folded conformation of the open chains in the confined space.⁹ When entrapped inside the confined space of the pore, the linear precursor would considerably reduce conformational flexibility to promote intramolecular cyclization. Moreover, sequestering the end-functionalized substrates inside the hydrophobic cavity prohibits any possibilities for undesired intermolecular oligomerization. The coupling reaction of a similarly sized R2 without branched alkyl chains also undergoes nearly perfect cyclization, indicating that the compatible size of the precursors to the internal cavities rather than molecular structure plays a pivotal role in clean cyclization (Figures S9 and S22). This is further supported by the identical experiments with a smaller substrate, R3, and a larger substrate, R4, which are not compatible to the internal cavities for binding, thus unable to be cyclized using the porous nanosheets (Table S3). Subsequently, when the porous nanosheet materials are added to a mixture solution of R1, R3, and R4, the cyclization yielded only P1 (Figure 4d), demonstrating that our single-layered porous materials are able to perform selective cyclization of only a trapped open chain among the mixed substrates of different sizes. To extend the scope of the cyclization reaction in the porous sheets, we have performed metal-free Knoevenagel condensation with an analogous linear substrate, which showed perfect macrocyclization within 80 min at room temperature (Figures S7, S10, and S23).

Spontaneous Release of the Macrocycles. Notably, when the substrate conversion is completed, the macrocycle product is spontaneously released out of the porous materials to precipitate without applying any external forces such as shaking and stirring (Figures S24 and S25). After removal of the precipitated macrocycle product by decanting, analytical HPLC measurements of the solution showed a complete lack of the cyclic product (Figure S26), demonstrating that converting into a macrocycle leads the substrate to

spontaneously release out of the internal pores. The release experiments showed that the macrocycle is completely released over an additional 8 h of standing (Figure 5a). This is in sharp

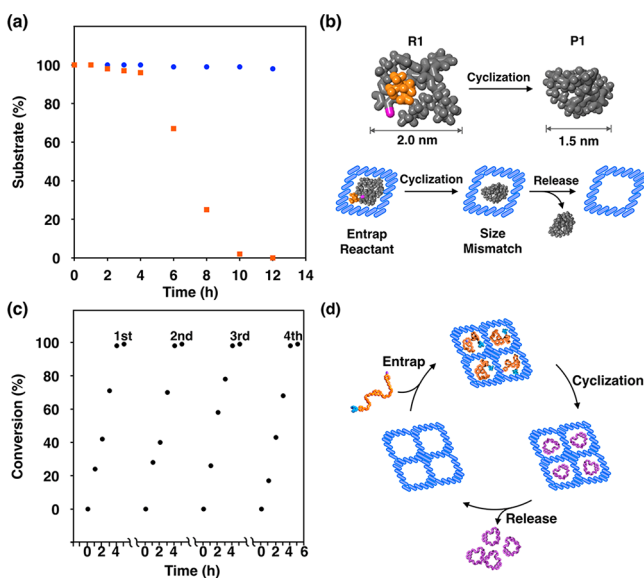


Figure 5. Spontaneous release of a macrocycle product and repeated cycles. (a) Substrate amount remaining in the porous nanosheets of **1** in the presence of Pd (0) (orange ■) and in the absence of Pd (0) (blue ●) with time variation. (b) Top: molecular sizes of **R1** and **P1** determined by molecular dynamic simulations in water. Bottom: schematic representation of spontaneous release of products after macrocyclization due to size mismatch between the internal cavity and the cyclized product. (c) Repeated cycles of HPLC conversions of **R1** as a function of time. (d) Schematic representation of repeated cycles of entrapping linear precursors, cyclization, and spontaneous release of macrocycle products.

contrast to the linear substrate which resides inside the pore during this period of time without any noticeable release (Figure 5a). The spontaneous release could be attributed to the size mismatch of the substrate with the fixed internal cavity by changing into a cyclic structure with decreasing hydrodynamic volume (Figures S27 and S28). Macrocycle structures possess smaller hydrodynamic volumes in comparison to their linear counterparts as a consequence of a conformational constraint of cyclic chains.³³ Considering that the substrates adopt a constrictive conformation in a poor solvent together with decreasing molecular weight after cyclization, molecular simulations showed that the cyclization of **R1** leads to considerable size reduction from 2.0 to 1.5 nm in diameter (Figure 5b and Figure S19), implying considerable size mismatch between the internal cavity ($d \approx 2.2$ nm) and the cyclized product. Hence, the cyclized substrate would no longer fit into the internal cavity, which is then spontaneously released out of the pore interior. This is supported by additional uptake experiments with presynthesized **P1**, which showed that the cyclic molecule is incapable of binding to the internal cavity (Figure S29). This result suggests that the chemical transformation of the substrate would modulate binding affinity with the pore walls through size reduction, thus being released as a product from the internal cavity, which is spontaneously separated from the solution by precipitation. As a result, the conversion of the substrate inside the cavity enables the porous materials to spontaneously release the

product, reminiscent of enzymatic action that changes a substrate to release as a product.³⁴

Repeated Macrocyclization. Considering the spontaneous release of the macrocycle product to precipitate, the porous nanosheet solution is able to carry out a new cycle of binding substrates to convert into macrocycles and then release (Figure 5c). Indeed, upon subsequent addition of **R1** into the supernatant solution after removal of the precipitated product by decanting, a new cycle of the substrate conversion takes place without compromising the pore performance in both uptake and conversion efficiency (Table S4 and Figures S30 and S31). The subsequent cycles showed that the porous nanosheet materials repeatedly perform full conversion and complete release up to 4 cycles, demonstrating that the pores are highly stable without deterioration in their performance even after many cycles of binding the substrate for conversion. The stability of the porous materials was further confirmed by X-ray scatterings and TEM after 4 cycles of these performances (Figures S32 and S33). The results showed that the original porous nanosheet structures are retained without any structural deformation, indicative of high stability over repeated cyclization performance.

CONCLUSION

Our results show that the single-layered porous nanostructures allow repetitive generation of macrocycles through repeated cycles of substrate catch without deterioration in pore performance (Figure 5d). This is attributed to the fact that the single-layered 2D assembly enables all the pores to bind the linear substrate inside discrete cavities to adopt a constrictive conformation, to facilitate clean cyclization, and to spontaneously release the substrate after conversion. The regenerated porous nanosheets with hollow cavities after self-separation of the product perform consecutive cycles of binding the substrate for cyclization and spontaneous release. The crystalline packing of **1** into the 2D frameworks seems to play an important role, not only in pore stability for repeated performance without deterioration but also in the fixed internal cavity enabling the spontaneous release of the substrates after conversion. In most cases, molecular containers with a flexible size bind products as efficiently as substrates, thereby inhibiting spontaneous release and recycles.³⁵ Although extended porous materials with fixed, open channels may function as a molecular container performing cyclization in a confined space, the cavities are inadequate to completely sequester linear substrates for clean intramolecular cyclization because the hollow cavities are not uniformly discrete.²⁵ Considering their compartmentalized structures, exfoliated porous layers could be suitable for sequestering precursor molecules; however, the layer thickness of sub-nanometer scales is insufficient for in-plane pores to restrict open chains with a folded conformation for cyclization.^{20–23} Therefore, the notable feature of our porous nanosheets is their ability to sequester linear substrates inside confined spaces with nearly perfect uptake to perform clean cyclization. In combination with the self-separation capability, the sequestration feature of open precursors within confined spaces enables the porous materials to act as a highly efficient macrocycle generator, performing consecutive cycles of changing a linear substrate to release as a macrocycle through repeated substrate catch. Thereby, our results exemplify that a simple catch-and-release purification strategy can translate into extended porous nanomaterials to create a powerful macrocycle generator.³⁶

We anticipate that such a strategy will provide a new insight into automated reaction machines capable of addressing complex sorting and reaction problems,³⁷ and reactor membranes for diverse chemical conversions enabling self-generation and self-separation of the products on passing across their internal cavities.

■ ASSOCIATED CONTENT

Supporting Information

The Supporting Information is available free of charge at <https://pubs.acs.org/doi/10.1021/jacs.9b11004>.

Experimental procedures, synthesis of molecules, NMR data, MALDI-TOF data, spectroscopy data, HPLC data, and TEM images (PDF)

■ AUTHOR INFORMATION

Corresponding Author

Myongsoo Lee – Jilin University, Changchun, China;
 orcid.org/0000-0002-5315-3807; Email: mslee@jlu.edu.cn

Other Authors

Xin Liu – Jilin University, Changchun, China
Xiaobin Zhou – Jilin University, Changchun, China
Bowen Shen – Jilin University, Changchun, China
Yongju Kim – Korea University, Seoul, Korea
Huaxin Wang – Jilin University, Changchun, China
Wanting Pan – Jilin University, Changchun, China
Jehan Kim – Pohang Accelerator Laboratory, Postech, Pohang, Korea

Complete contact information is available at:
<https://pubs.acs.org/doi/10.1021/jacs.9b11004>

Author Contributions

[¶]X.L. and X.Z. contributed equally.

Notes

The authors declare no competing financial interest.

■ ACKNOWLEDGMENTS

This work was supported by the National Natural Science Foundation of China (21634005 and 51473062).

■ REFERENCES

- (1) White, C. J.; Yudin, A. K. Contemporary strategies for peptide macrocyclization. *Nat. Chem.* **2011**, *3*, 509–524.
- (2) Driggers, E. M.; Hale, S. P.; Lee, J.; Terrett, N. K. The exploration of macrocycles for drug discovery — an underexploited structural class. *Nat. Rev. Drug Discovery* **2008**, *7*, 608–624.
- (3) Schappacher, M.; Deffieux, A. Synthesis of macrocyclic polymer brushes and their self-assembly into supramolecular tubes. *Science* **2008**, *319*, 1512–1515.
- (4) Marti-Centelles, V.; Pandey, M. D.; Burguete, M. I.; Luis, S. V. Macrocyclization reactions: the importance of conformational, configurational, and template-induced preorganization. *Chem. Rev.* **2015**, *115*, 8736–8834.
- (5) Oueis, E.; Jaspars, M.; Westwood, N. J.; Naismith, J. H. Enzymatic macrocyclization of 1,2,3-triazole peptide mimetics. *Angew. Chem., Int. Ed.* **2016**, *55*, 5842–5845.
- (6) Takezawa, H.; Kanda, T.; Nanjo, H.; Fujita, M. Site-selective functionalization of linear diterpenoids through U-shaped folding in a confined artificial cavity. *J. Am. Chem. Soc.* **2019**, *141*, 5112–5115.

- (7) Wang, Q.-Q.; Gonell, S.; Leenders, S. H. A. M.; Dürr, M.; Ivanović-Burmazović, I.; Reek, J. N. H. Self-assembled nanospheres with multiple endohedral binding sites pre-organized catalysts and substrates for highly efficient reactions. *Nat. Chem.* **2016**, *8*, 225–230.
- (8) Hart-Cooper, W. M.; Clary, K. N.; Toste, F. D.; Bergman, R. G.; Raymond, K. N. Selective monoterpene-like cyclization reactions achieved by water exclusion from reactive intermediates in a supramolecular catalyst. *J. Am. Chem. Soc.* **2012**, *134*, 17873–17876.
- (9) Mosca, S.; Yu, Y.; Gavette, J. V.; Zhang, K.-D.; Rebek, J., Jr. A deep cavitand templates lactam formation in water. *J. Am. Chem. Soc.* **2015**, *137*, 14582–14585.
- (10) Lee, T.-C.; Kalenius, E.; Lazar, A. I.; Assaf, K. I.; Kuhnert, N.; Grün, C. H.; Jänis, J.; Scherman, O. A.; Nau, W. M. Chemistry inside molecular containers in the gas phase. *Nat. Chem.* **2013**, *5*, 376–382.
- (11) Kaphan, D. M.; Toste, F. D.; Bergman, R. G.; Raymond, K. N. Enabling new modes of reactivity via constrictive binding in a supramolecular-assembly-catalyzed aza-prinscyclization. *J. Am. Chem. Soc.* **2015**, *137*, 9202–9205.
- (12) Houk, K. N.; Leach, A. G.; Kim, S. P.; Zhang, X. Binding affinities of host-guest, protein-ligand, and protein-transition-state complexes. *Angew. Chem., Int. Ed.* **2003**, *42*, 4872–4897.
- (13) Wang, K.; Cai, X.; Yao, W.; Tang, D.; Kataria, R.; Ashbaugh, H. S.; Byers, L. D.; Gibb, B. C. Electrostatic control of macrocyclization-reactions within nanospaces. *J. Am. Chem. Soc.* **2019**, *141*, 6740–6747.
- (14) Slater, A. G.; Cooper, A. I. Function-led design of new porous materials. *Science* **2015**, *348*, aaa8075-1–aaa8075-10.
- (15) Mitra, T.; Jelfs, K. E.; Schmidtman, M.; Ahmed, A.; Chong, S. Y.; Adams, D. J.; Cooper, A. I. Molecular shape sorting using molecular organic cages. *Nat. Chem.* **2013**, *5*, 276–281.
- (16) Percec, V.; Dulcey, A.; Balagurusamy, V. S. K.; Miura, Y.; Smidrkal, J.; Peterca, M.; Nummelin, S.; Edlund, U.; Hudson, S. D.; Heiney, P. A.; Duan, H.; Magonov, S. N.; Vinogradov, S. A. Self-assembly of amphiphilic dendritic dipeptides into helical pores. *Nature* **2004**, *430*, 764–768.
- (17) Kaucher, M. S.; Peterca, M.; Dulcey, A. E.; Kim, A. J.; Vinogradov, S. A.; Hammer, D. A.; Heiney, P. A.; Percec, V. Selective transport of water mediated by porous dendritic dipeptides. *J. Am. Chem. Soc.* **2007**, *129*, 11698–11699.
- (18) Barboiu, M. Artificial Water channels-incipient innovative developments. *Chem. Commun.* **2016**, *52*, 5657–5665.
- (19) Sun, B.; Kim, Y.; Wang, Y.; Wang, H.; Kim, J.; Liu, X.; Lee, M. Homochiralporous nanosheets for enantiomer sieving. *Nat. Mater.* **2018**, *17*, 599–604.
- (20) Peng, Y.; Li, Y.; Ban, Y.; Jin, H.; Jiao, W.; Liu, X.; Yang, W. Metal-organic framework nanosheets as building blocks for molecular sieving membranes. *Science* **2014**, *346*, 1356–1359.
- (21) Kissel, P.; Murray, D. J.; Wulfange, W. J.; Catalano, V. J.; King, B. T. A Nanoporous two-dimensional polymer by single-crystal-to-single-crystal photopolymerization. *Nat. Chem.* **2014**, *6*, 774–778.
- (22) Xu, H.; Gao, J.; Jiang, D. Stable, crystalline, porous, covalent organic frameworks as a platform for chiral organocatalysts. *Nat. Chem.* **2015**, *7*, 905–912.
- (23) Zhang, K.-D.; Tian, J.; Hanifi, D.; Zhang, Y.; Sue, A. C.-H.; Zhou, T.-Y.; Zhang, L.; Zhao, X.; Liu, Y.; Li, Z.-T. Toward a single-layer two-dimensional honeycomb supramolecular organic framework in water. *J. Am. Chem. Soc.* **2013**, *135*, 17913–17918.
- (24) Kim, Y.; Shin, S.; Kim, T.; Lee, D.; Seok, C.; Lee, M. Switchable nanoporous sheets by the aqueous self-assembly of aromatic macrobicycles. *Angew. Chem., Int. Ed.* **2013**, *52*, 6426–6429.
- (25) Dong, R.; Zhang, T.; Feng, X. Interface-assisted synthesis of 2D materials: trend and challenges. *Chem. Rev.* **2018**, *118*, 6189–6235.
- (26) Huang, Z.; Kang, S.-K.; Banno, M.; Yamaguchi, T.; Lee, D.; Seok, C.; Yashima, E.; Lee, M. Pulsating tubules from non-covalent macrocycles. *Science* **2012**, *337*, 1521–1526.
- (27) Förster, S.; Plantenberg, T. From self-organizing polymers to nanohybrid and biomaterials. *Angew. Chem., Int. Ed.* **2002**, *41*, 688–714.

(28) Wu, X.; Han, X.; Liu, Y.; Liu, Y.; Cui, Y. Control interlayer stacking and chemical stability of two-dimensional covalent organic frameworks via steric tuning. *J. Am. Chem. Soc.* **2018**, *140*, 16124–16133.

(29) Montes-Navajas, P.; Corma, A.; Garcia, H. Complexation and fluorescence of tricyclic basic dyes encapsulated in cucurbiturils. *ChemPhysChem* **2008**, *9*, 713–720.

(30) Liu, J.; Jiang, N.; Ma, J.; Du, X. Insight into unusual downfield NMR shifts in the inclusion complex of acridine orange with cucurbit[7]uril. *Eur. J. Org. Chem.* **2009**, *2009*, 4931–4938.

(31) Zhou, H.; Zhao, Y.; Gao, G.; Li, S.; Lan, J.; You, J. Highly selective fluorescent recognition of sulfate in water by two rigid tetrakisimidazoliummacrocycles with peripheral chains. *J. Am. Chem. Soc.* **2013**, *135*, 14908–14911.

(32) Wu, S.; Li, Y.; Xie, S.; Ma, C.; Lim, J.; Zhao, J.; Kim, D. S.; Yang, M.; Yoon, D. K.; Lee, M.; Kim, S. O.; Huang, Z. Supramolecular nanotubes as a catalytic regulator for palladium cations: applications in selective catalysis. *Angew. Chem., Int. Ed.* **2017**, *56*, 11511–11514.

(33) Williams, R. J.; Dove, A. P.; O'Reilly, R. K. Self-assembly of cyclic polymers. *Polym. Chem.* **2015**, *6*, 2998–3008.

(34) Küchler, A.; Yoshimoto, M.; Luginbühl, S.; Mavelli, F.; Walde, P. Enzymatic reactions in confined environments. *Nat. Nanotechnol.* **2016**, *11*, 409–420.

(35) López-Vidal, E. M.; Fernández-Mato, A.; García, M. D.; Pérez-Lorenzo, M.; Peinador, C.; Quintela, J. M. Metallacycle-catalyzed S_N2 reaction in water: supramolecular inhibition by means of host-guest complexation. *J. Org. Chem.* **2014**, *79*, 1265–1270.

(36) Liu, Y.-S.; Zhao, C.; Bergbreiter, D. E.; Romo, D. Simultaneous deprotection and purification of BOC-amines based on ionic resin capture. *J. Org. Chem.* **1998**, *63*, 3471–3473.

(37) Li, J.; Ballmer, S. G.; Gillis, E. P.; Fujii, S.; Schmidt, M. J.; Palazzolo, A. M. E.; Lehmann, J. W.; Morehouse, G. F.; Burke, M. D. Synthesis of many different types of organic small molecules using one automated process. *Science* **2015**, *347*, 1221–1226.